Kink-pair nucleation on dislocations under stress in the two-dimensional Frenkel-Kontorova model

David Rodney[1] and Laurent Proville[2]
[1]*SIMAP-GPM2, Grenoble INP, CNRS/UJF, 38402 Saint Martin d'Hères, France*
[2]*CEA, DEN, Service de Recherches de Métallurgie Physique, F-91191 Gif-sur-Yvette, France*
(Received 30 June 2008; published 24 September 2008)

We present static and dynamic simulations to study the thermally activated motion of dislocations. The model employed is the two-dimensional Frenkel-Kontorova model. The main interest is to allow simulations of dislocation dynamics over long-time periods (~600 ns), giving access to large ranges of applied stresses and temperatures. The kink-pair nucleation rates, determined from dynamical simulations, are studied as a function of the ratio between the kink-pair activation enthalpy and the thermal energy. The former is computed from static simulations based on the elastic nudged band method. We show here that the dislocation motion is composed of two regimes: a low-temperature regime where the nucleation rate follows a thermally activated exponential law and a high-temperature regime where the motion is slower than expected from the low-temperature exponential law. We evidence a correlation between successive dislocation jumps that stems from the dynamics of internal modes of the dislocation and impedes high-frequency nucleation events.

DOI: 10.1103/PhysRevB.78.104115 PACS number(s): 62.20.F−, 05.40.−a

I. INTRODUCTION

Due to the discrete nature of crystals, dislocations experience a lattice resistance materialized by the Peierls stress, i.e., the minimum resolved shear stress (RSS) required to move a dislocation from one stable position, a Peierls valley,[1] to the next without the help of thermal fluctuations. The Peierls stress depends on the nature of the interatomic bonds and on the dislocation core structure.[2,3] It can be as high as 0.5% of the shear modulus, for example in covalent semiconductors where dislocation motion requires bond swapping[4] and in body-centered-cubic (bcc) crystals where screw dislocations have a nonplanar core structure.[5,6] When the applied RSS is below the Peierls stress, dislocation glide is helped by thermal fluctuations. It proceeds from the thermally activated nucleation of kink pairs that brings a dislocation segment into the next Peierls valley.[7] The subsequent propagation of the kinks along the dislocation line progressively transfers the rest of the dislocation into the new Peierls valley.

The rate of kink-pair nucleation has been studied mainly in the context of the (1+1)-dimensional soliton-bearing theories:[8] the continuous sine-Gordon (SG) theory,[9–13] its discrete Frenkel-Kontorova analog,[14,15] and the $\phi^2-\phi^4$ theory.[16,17] The activation enthalpy H of the critical kink-pair nucleus was obtained analytically for the SG theory.[9,10] The nucleation rate Γ was also expressed but only in the limit of strong damping and weak external force.[11,18] To our knowledge, such predictions have been confirmed by computer simulations only in the equilibrium case when no stress is applied and led to some debate due to the difficulty to compute the nucleation rate directly in the simulations.[16,17,19,20] From the same type of model representing an elastic string moving on a nonlinear substrate potential, early theories were also devised in the field of dislocation physics,[21,22] where an activation law $\Gamma \propto \sqrt{1/k_BT}\exp(-H/k_BT)$ was predicted in agreement with the analytical works mentioned above. The particular temperature dependence of the pre-exponential factor stems from the Goldstone mode[23] of the kink-pair saddle configuration.

Three-dimensional (3D) molecular-dynamics (MD) simulations at finite temperature have been applied to study the thermally activated glide of dislocations.[24–27] Atomistic computations of dislocation static properties such as the Peierls stress,[28,29] the kink width,[30,31] and kink-antikink interaction[32,33] are of prominent interest to improve our understanding of metal plasticity. Such 3D simulations allow a realistic representation of the atomistic structure but imply too many degrees of freedom to reach long enough simulated time scales to extract statistically relevant information for a broad range of stress and temperature.

Our aim in the present paper is to study the rate of kink-pair nucleation as a function of temperature and stress. In order to simulate sufficiently long-time scales, we have chosen to work at the frontier between the atomic-scale simulations and the SG scalar field theory. We employ the two-dimensional (2D) Frenkel-Kontorova (FK) model proposed by Gornostyrev *et al.*[34,35] In comparison with (1+1)D theories, the 2D-FK model provides a better account for the atomic-scale dislocation core structure. The dislocation thermal bath is also more realistic than the conventional SG Langevin thermostat since the 2D-FK lattice implies that 2D phonons scatter on the dislocation. The main differences between the 2D-FK model and a fully atomistic 3D simulation are that: (i) a phenomenological substrate potential is introduced to model the dislocation glide plane relief and (ii) the kink-antikink interaction decays exponentially with the separation distance, whereas a 3D elastic medium yields a Coulomb-type potential.[21,36] Such simplifications, also present in the SG model, are the necessary requirements for speeding up the simulations. Dynamical simulations at finite temperature are used to evaluate the kink-pair nucleation rate as a function of external stress and temperature. The kink-pair activation enthalpy H is computed independently using the static nudged elastic band (NEB) method[37] coupled to a standard NEWTON-RAPHSON (NR) algorithm[38] to ensure final

convergence to the kink-pair saddle state. We demonstrate numerically the emergence of two regimes at low and high temperatures. At low temperature, the kink-pair nucleation rate Γ follows the prediction of a transition state theory[39] with an athermal prefactor $\Gamma=\Gamma_0 \exp(-H/k_BT)$. The Goldstone term is shown to provide only a small correction to the above expression. An athermal pre-exponential factor corresponds to the vibration of an elementary segment of dislocation at the bottom of its Peierls valley. Such expression was proposed independently for the thermal activation of dislocation glide by Seeger[7] and Friedel.[40] At high temperature, but still with $k_BT<H$, the nucleation rate averaged over long simulations becomes smaller than expected from the low-temperature exponential law. The slowing down implied by the Goldstone term in that temperature range can not account for the strong effect revealed here. Instead, we show by studying the vibrational modes of the dislocation that the origin of the high-temperature regime is a recovery process that occurs inside the dislocation core after kink-antikink collisions.

In Sec. II, we recall the formalism of the 2D Frenkel-Kontorova model. Our static simulations to determine the kink-pair activation enthalpy as a function of the applied stress are reported in Sec. III. The dynamical simulation data are presented and interpreted in Sec. IV. In Sec. V, our end results are discussed and compared to experiments and other thermally activated models for the dislocation glide.

II. COMPUTATIONAL MODEL

As proposed in Refs. 34 and 35 and illustrated in Fig. 1(a), we consider a hexagonal plane of atoms linked between first neighbors by springs and subjected to a periodic potential. The potential energy is written as

$$E=\frac{K}{2}\sum_{\langle n,m\rangle}(\mathbf{u_n}-\mathbf{u_m})^2+P\sum_n\sum_{\mathbf{g}}[1-\cos(\mathbf{g}\cdot\mathbf{u})]-\sum_n F_y u_n^y, \tag{1}$$

where $\mathbf{u_n}$ is the displacement of atom n with respect to its position in the perfect hexagonal lattice and $\langle n,m\rangle$ designates first neighbor pairs. The stiffness of the interatomic bonds is K. A sinusoidal substrate potential (of depth P) is used with $\mathbf{g_1}=(4\pi/\sqrt{3}a)(1;0)$ and $\mathbf{g_{2,3}}=(4\pi/\sqrt{3}a)(1/2;\pm\sqrt{3}/2)$, which are the reciprocal hexagonal lattice vectors of minimum length. The lattice parameter is noted as a. A shear stress σ (force per atomic area) may be applied in direction Y by adding to each atom an external force $F_y=\sigma a^2\sqrt{3}/2$. Periodic boundary conditions are applied in directions X and Y.

A screw dislocation is introduced by displacing all atoms in the left half of the plane (region $X<0$) by a in direction Y and relaxing the system to a minimum-energy configuration. To account for the presence of the dislocation, the periodic boundary conditions in direction X are shifted by a in direction Y; i.e., atoms leaving the cell from the $X>0$ ($X<0$) side are reintroduced on the $X<0$ ($X>0$) side after a rigid displacement $-a$ ($+a$) in direction Y. Figure 1 shows an example of relaxed atomic configuration near a dislocation line. The Peierls valleys for this dislocation correspond to atomic

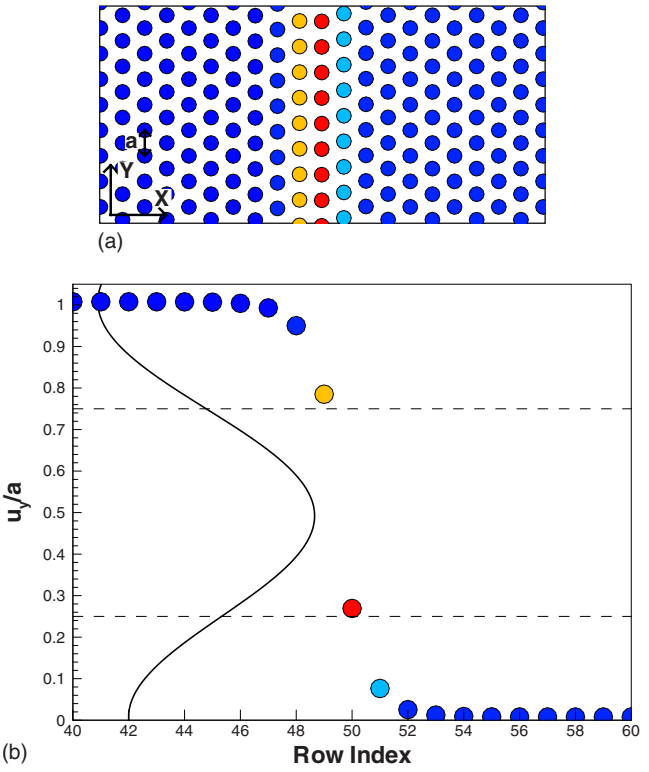

FIG. 1. (Color online) Atomic configuration near a dislocation line with $Ka^2/P=18.35$ and $\sigma/\sigma_P=0.41$. The colors depend on the potential energy. In (a), the cell is seen from above. In (b), atomic displacements in direction Y are shown as a function of the position in direction X expressed by the corresponding row index. The solid curve in (b) is the substrate potential energy as a function of u_y assuming $u_x=0$. The energy scale is arbitrary.

rows in direction Y. Their separation is $d=a\sqrt{3}/2$. The parameters of the model are adjusted to correspond to bcc iron. The lattice parameter is taken equal to the Burgers vector of this metal: $a=0.2473$ nm.[41] The parameter P is related to the shear modulus in direction Y by the linear elastic relation

$$\mu=\frac{1}{V_{\mathrm{at}}}\frac{\partial^2 E/N}{\partial\epsilon^2}\bigg|_{\epsilon=0}=\frac{8P\pi^2}{a^2 d}, \tag{2}$$

where $\epsilon=u_y/a$ is the shear deformation, $V_{\mathrm{at}}=a^2d$ is the atomic volume, and E/N is the potential energy per atom. With $\mu=116$ GPa,[41] we obtain $P=0.12$ eV. The remaining parameter K, or more precisely the ratio Ka^2/P, measures the strength of the interatomic bonds with respect to the substrate potential. It directly controls the width of the dislocation core, the Peierls stress for rigid motion, and the kink-pair activation energy. The Peierls stress is determined by increasing the applied stress incrementally on a straight dislocation and minimizing the potential energy for each increment until the dislocation is set in motion. Figure 2 shows the evolution of the Peierls stress for rigid motion as a function of Ka^2/P. In the following, we use $Ka^2/P=18.35$ which yields a Peierls stress of 2175 MPa. This value of the Peierls stress is higher than in 3D models (see Refs. 24–27), but it is required in order to have a high enough kink-pair formation energy, equal to 0.417 eV for the present value of Ka^2/P, to

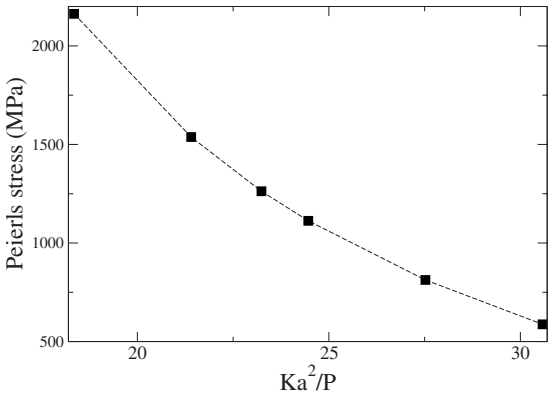

FIG. 2. Peierls stress for rigid motion as a function of Ka^2/P. The dashed line is a guide for the eyes.

study the kink-pair nucleation rate over a wide range of stresses. Gornostyrev *et al.*[34] used lower values of this parameter, $Ka^2/P=8.33$ and 12.5, with therefore narrower dislocation cores and higher Peierls stresses. The dislocation core corresponding to our parameters is shown in Fig. 1(b). The dislocation core extent is narrow since the displacement goes from $0.95a$ to $0.05a$ within three Peierls valleys, which is consistent with the small extension of the screw dislocation core in bcc iron.

For the simulations at finite temperature, Newton's equations of motion are integrated using the velocity VERLET algorithm[42] with a 1 fs time step. Since in 3D-MD simulations of dislocation dynamics no thermostat is usually used,[24–27] we applied a weak thermostat based on ANDERSEN algorithm,[43] whereby the particles are randomly assigned a new velocity component in direction X or Y taken from a Maxwellian distribution, with an average frequency $\eta=0.001$. We checked that the results discussed below are independent of this choice by performing test simulations with $\eta=0.01$ and other types of thermostat as the Brownian dynamics used in Refs. 34 and 35. The insensitivity of the results on the external thermostat shows that the thermalization of the dislocation proceeds mainly throughout the atomic lattice phonon scattering as usually recognized in the dislocation theory[21,44] and 3D-MD simulations.

In order to evaluate precisely kink-pair nucleation rates, we modeled a short dislocation such that at any moment, there is at most one kink-pair on the dislocation line. The lattice is made of $N_x=100$ rows (Peierls valleys) of $N_y=50$ atoms. The position of the dislocation X_D is expressed as the number of rows over which the dislocation has glided. It is mathematically written as

$$X_D = \frac{\sum_n \mathrm{nint}(u_n^y/a)}{N_y}, \tag{3}$$

where $\mathrm{nint}(x)$ is the closest integer to x. In the range of temperatures and applied stresses considered here, the motion of the dislocation is intermittent with waiting periods separated by the nucleation of kink-pairs. The kink and antikink then travel along the dislocation in opposite directions and when they meet through the periodic boundary conditions, their interaction is always destructive. No back and forth motions were detected in our simulations where the kink-pairs systematically form in the direction of the external force. Note that as the temperature increases, multiple kink-pairs are observed, i.e., a second kink-pair nucleates on an expanding one. This is reminiscent of avalanches due to inertial effects.[26] However, these avalanches contain rarely more than two kink-pairs and are counted as single nucleation events. The simulations were used to extract distributions of waiting times. The latter is defined as continuous periods of time over which X_D remains equal to an integer value with a maximum deviation $\delta=0.05$. δ has been chosen such that to ensure, once it is detected, a nucleation event leads systematically to kink-pair expansion and relaxation of the whole dislocation at the bottom of the next-nearest Peierls valley. With such methodology, the duration of kink-pair expansion is not counted in the statistics. The distributions of waiting times were then used to compute the average waiting time $\langle t_w \rangle$ and its reciprocal average nucleation rate Γ. Since $\langle t_w \rangle$ strongly depends on the temperature, the duration of the simulations varied from 50 ns at the highest temperatures to 600 ns at the lowest, in order to maintain small statistical errors.

III. STATIC SIMULATIONS

We computed the activation enthalpy for kink-pair nucleation as a function of applied stress using the NEB method.[37] A path is constructed between a product (the dislocation relaxed in a Peierls valley) and a reactant (the dislocation is relaxed in the next valley) by forming a chain of replicas of the system linked in phase space by linear springs. A minimum energy path (MEP) is obtained by minimizing the total energy of the replicas perpendicularly to the local tangent of the path while allowing the replicas to move along the path by relaxing the spring forces. We used 20 replicas and a spring constant $K_{\mathrm{NEB}}=0.1$ eV Å^{-2}. The initial path was taken in the form of a kink-pair that progressively expands along the dislocation line. The same method has been used in 3D simulations in bcc iron[45] and fcc aluminum.[27] In order to reduce the error yielded through the NEB spring forces, we apply a NR method[38] starting from the NEB replica closest to the extremum along the MEP, which allows us to obtain a satisfactory computation of the kink-pair saddle configuration.

The computed activation enthalpy H is computed as a function of the external stress. Results are reported in Fig. 3 where H has been scaled by the formation energy $H_{\mathrm{KP}}=0.417$ eV of a kink-pair in absence of applied stress. The latter is computed independently by relaxing under zero stress a dislocation containing a far apart kink and antikink. The solid line in Fig. 3 is the prediction of the SG model[47] that is well fitted by the analytical expression proposed by Kocks[48] and used by Tang *et al.*[49]

$$\frac{H(\sigma)}{H_{\mathrm{KP}}} = \left[1 - \left(\frac{\sigma}{\sigma_P}\right)^p\right]^q \tag{4}$$

with adjusted parameters $p=0.8$ and $q=1.286$. For comparison and further discussions, we added in Fig. 3 the experi-

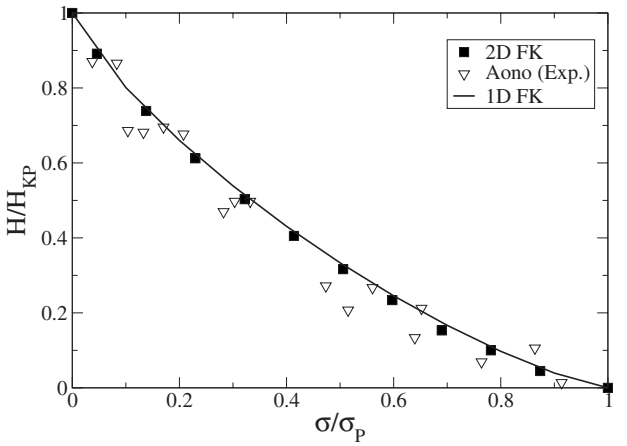

FIG. 3. Activation enthalpy H for kink-pair nucleation as a function of applied stress σ normalized by the Peierls stress (σ_P =2175 MPa). The enthalpy has been normalized by the kink-pair formation energy (H_{KP}=0.417 eV). The solid line corresponds to the (1+1)D-SG model data fitted by the Kocks law [see Eq. (4)]. Open triangles are experimental results obtained on bcc iron (Ref. 46).

mental data obtained by Aono *et al.*[46] in bcc iron. The motion of the screw dislocation from one Peierls valley to the next implies an increase in the Y displacement in each row. More precisely, with the notation of Fig. 1(b), the displacement in a row of index n increases to become equal to the initial displacement in row $n-1$. In Fig. 1(b), the row that is mostly affected in this process is row 50 where the displacement in direction Y increases from about $0.25a$ to about $0.75a$ to become equal to the initial displacement of row 49. Figure 4 shows the atomic displacement in different rows along the screw dislocation for activated states at low and high stresses obtained with the NEB. Note that the displacements shown here are in the Y direction, i.e., along the screw dislocation line. The activated state is essentially made of a local increase in the displacement of a group of atoms in row 50. The amplitude of the displacement in the nucleus decreases with increasing applied stress. At low stress [Fig. 4(a)], the displacement in the middle of the nucleus reaches about $0.75a$, i.e., almost the position of row 49, while at higher stress [Fig. 4(b)] the displacement extends only up to $0.5a$, which is the maximum of the substrate potential [see Fig. 1(b)]; i.e., the displacement above where the atoms are dragged toward the next energy minimum of the substrate energy. Note also that, as seen in Fig. 4, the nucleus is always made of less than ten atoms.

Once the kink-pair saddle configuration was determined through the NEB-NR method, we carried out the linear analysis of the configuration. The eigenvalues of the unstable kink-pair Hessian are plotted in Fig. 5 against the applied stress. For convenience, we only report the lower part of the spectrum. One notices at high stress a translational Goldstone mode with a zero eigenvalue. For small external stresses, the translational invariance is broken by the emergence of a small secondary Peierls barrier, which forbids the kinks to move freely along the dislocation line. The same is found in the (1+1)D-FK model when the interatomic coupling is small enough. In the following, we will show that this Goldstone mode has only a weak influence on the dislocation dynamics studied here.

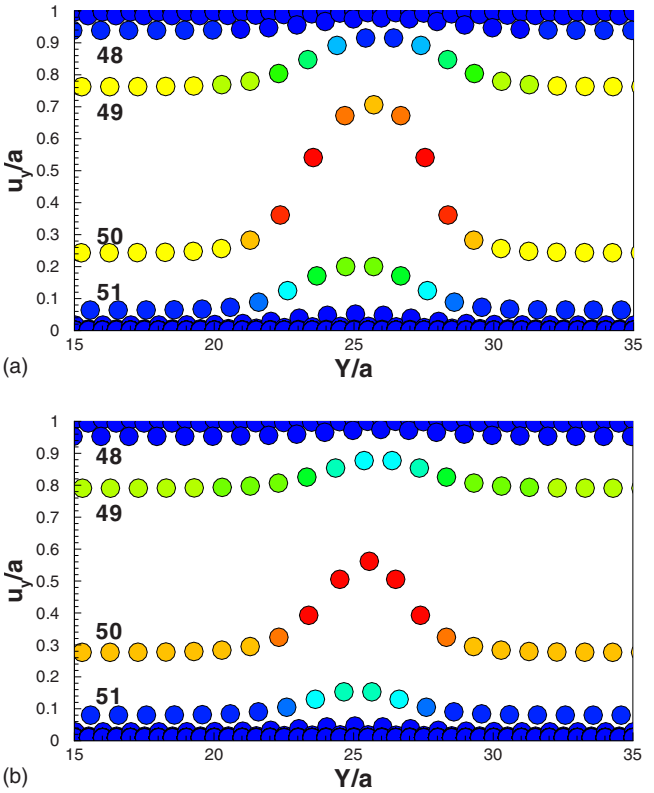

FIG. 4. (Color online) Activated configurations for (a) σ/σ_P =0.046 and (b) 0.41. Colors and row indexes correspond to Fig. 1(b).

IV. DYNAMICAL SIMULATIONS

We performed dynamical simulations at three applied stresses σ=700, 900, and 1100 MPa, i.e., σ/σ_P=0.32, 0.41, and 0.5 and temperatures varying from 100 to 350 K. Two

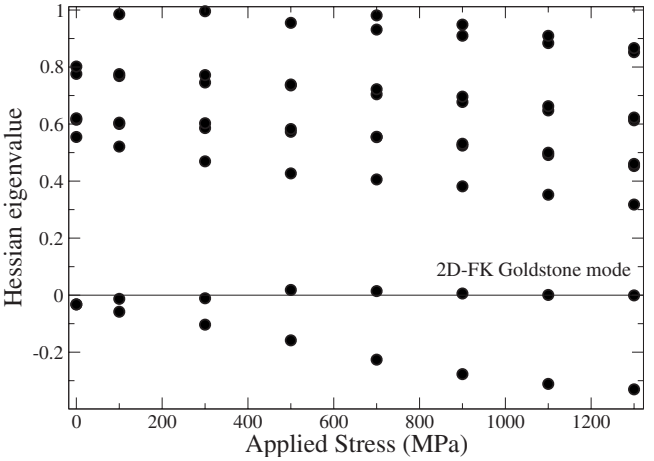

FIG. 5. Hessian eigenvalues of unstable kink-pair configurations as a function of applied stress.

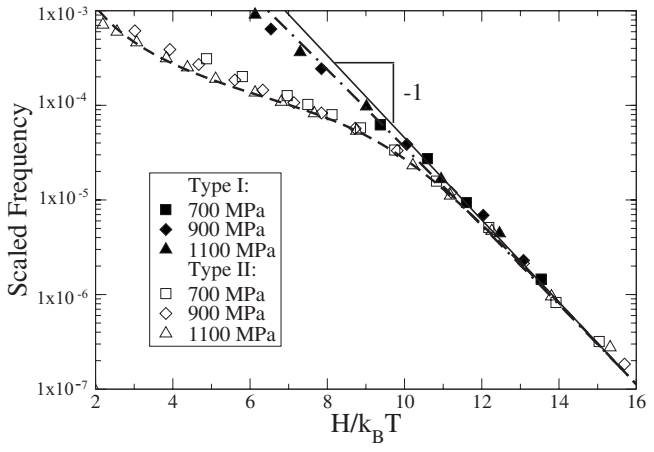

FIG. 6. Simulation data (symbols) for the normalized nucleation rate as a function of activation ratio H/k_BT. Filled symbols correspond to the statistics of first nucleations (type I simulations) while open symbols correspond to continuously recorded statistics (type II simulations). The solid line is the exponential law [Eq. (6)], the dot-dashed line the exponential law with a Goldstone prefactor [Eq. (7)], and the dashed line is the modified law [Eq. (10)].

different types of simulations have been carried out to measure the average waiting time $\Gamma^{-1}=\langle t_w\rangle$ for kink-pair nucleation. In the first type, hereafter denoted as type I, we computed the distribution of waiting times for the first nucleation event by resetting the simulation to its initial configuration with a different Maxwellian velocity distribution after each nucleation. The second type of simulation, denoted as type II, consists of recording the waiting times on the fly, i.e., in the course of some long-time simulations without stopping and resetting the dislocation configuration after each event. The difference between type I and II simulations lies in the fact that type II simulations allow for correlations between successive dislocation jumps whereas type I simulations do not. The total number of measures has been chosen such that to reduce the sampling error to less than 5% on the mean waiting time. Figure 6 shows the average nucleation rate Γ for type I and type II simulations as filled and open symbols, respectively. The frequencies are scaled by the dislocation length $(L/a=N_y=50)$ and a characteristic frequency of atomic vibrations $\nu_D=10^{13}$ s^{-1},

$$\tilde{\Gamma}=\frac{\Gamma}{\nu_D}\frac{a}{L}=\frac{1}{\langle t_w\rangle\nu_D}\frac{a}{L}. \tag{5}$$

The nucleation rate is plotted as a function of the dimensionless *activation ratio* between the activation enthalpy $H(\sigma)$ and the thermal energy k_BT. The activation enthalpies used here were obtained from the static simulations discussed in Sec. III.

At low temperature, when $H/k_BT>10$, type I and type II simulations coincide and the nucleation rate follows an exponential law with an exponent −1. The nucleation rate is thus expressed as

$$\tilde{\Gamma}=\exp(-H/k_BT), \tag{6}$$

which corresponds exactly to the thermally activated law proposed by Friedel.[40]

By way of contrast, at higher temperature, when $H/k_BT<10$, type I and type II simulations strongly deviate. Type I simulations remain close to Eq. (6), while in type II simulations, the average nucleation rate becomes lower than the extrapolation from the low-temperature regime; i.e., the dislocation velocity is slower than expected from the exponential law. We checked that the glide mechanism does not change at high temperatures in type II simulations. It remains intermittent and proceeds from the nucleation and propagation of kink-pairs on the dislocation line. Also, the waiting times in the high-temperature regime are of the order of several tens of picosecond and thus remain two orders of magnitude longer than the atomic oscillation period of the order of 0.1 ps.

In Fig. 6, at high temperature, the type I simulations slightly deviate from the straight line with a slope −1. The main reason is the Goldstone mode evidenced in Fig. 5. With the following form for the nucleation rate:

$$\tilde{\Gamma}=\alpha_I\sqrt{\frac{1}{k_BT}}\exp(-H/k_BT), \tag{7}$$

and $\alpha_I^2=0.0106$ eV as an adjusted parameter, it is possible to approach type I simulation data as shown in Fig. 6 (dash-dotted curve). Note that the stress dependence of α_I usually predicted[21] is not visible here. Moreover, since the Goldstone term does not yield any remarkable transition with temperature, it can not be at the origin of the high-temperature regime for type II simulations.

In order to analyze further the high-temperature regime, we show in Fig. 7 two representative examples of distributions of waiting times recorded during type II simulations. At low temperature [Fig. 7(a)], the distribution is well described by the Poissonian distribution shown as a solid line;

$$\rho(t)=\frac{1}{\langle t_w\rangle}\exp\left(-\frac{t}{\langle t_w\rangle}\right). \tag{8}$$

In the low-temperature regime, kink-pair nucleation events are thus uncorrelated with a probability per unit time equal to the inverse of the average waiting time. At high temperature [Fig. 7(b)], the distribution is not Poissonian. It has a maximum with a decreasing probability for short waiting times. This suppression of the short waiting times in the distribution is responsible for the relative decrease, in Fig. 6, in the nucleation rate with respect to the low-temperature exponential law. The high-temperature regime is thus related to a high-frequency cutoff in the nucleation event; i.e., after a jump, there is an incubation time t_i during which the dislocation cannot undergo another jump. To tentatively explain the origin of such correlation between nucleation events, we studied the internal modes of the dislocation. This work is reported in the Appendix where, as in other studies,[34,35] dislocation modes are clearly identified. We noticed a delay in the relaxation of the atomic row in the dislocation core (row 50 in Fig. 1). Subsequently to the annihilation of a kink and its antikink, this core atomic row occupies an average position which remains behind its static equilibrium position. After a time period comparable to the maximum of the distribution function in Fig. 7(b), i.e., on the order of 10–20 ps,

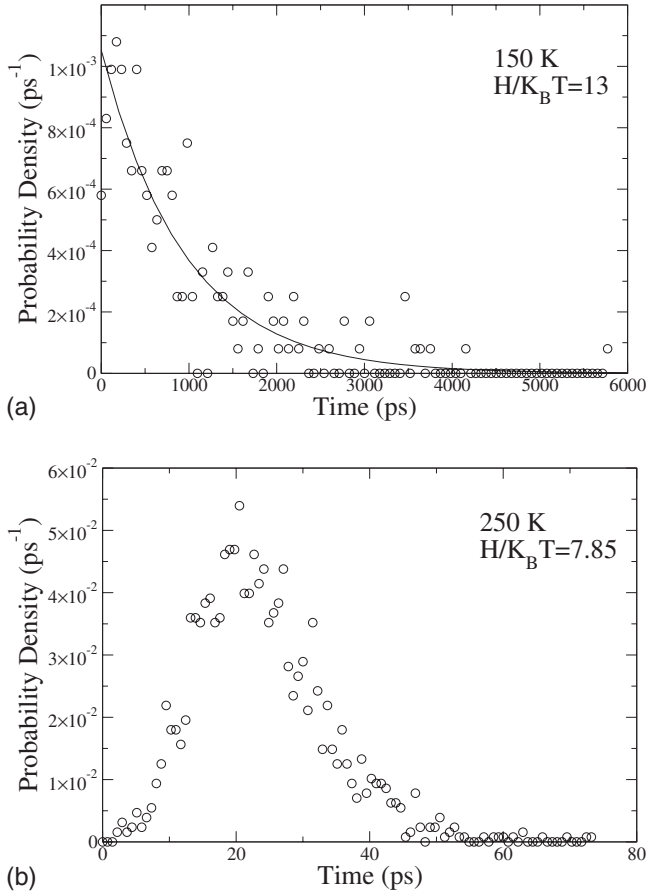

FIG. 7. Distribution of waiting times in type II simulations (see text) at 900 MPa and temperatures of (a) 150 and (b) 250 K. The solid line in (a) is the Poissonian distribution of Eq. (8) with $\langle t_w \rangle = 950$ ps.

the core atomic row recovers its static equilibrium position on average. We conclude that the time delay t_i for kink-pair incubation is related to a recovery process inside the dislocation core.

To rationalize the expression for t_i, we propose a phenomenological approach. We noted that the time delay is consecutive to a previous jump of the dislocation which terminates by a kink-antikink annihilation. The energy liberated through the kink collision is of the order or larger than the kink-pair formation enthalpy H. This energy is dissipated through dislocation radiation in the phonon bath. According to Leibfried,[50] the damping coefficient for a unitary dislocation segment is given by $\lambda = 3k_B T z / 20 c_s b^2$ where c_s is the transverse sound velocity, $b=a$ is the Burgers vector, and z the number of atoms per unit cell. Different authors (see Ref. 21 and references therein) derived other expressions for the various processes at play during dislocation thermalization, but the proportionality to $k_B T$ was present in all the different works. Since we are primarily interested in the temperature dependence, we keep this ingredient of the dislocation-phonon-scattering theory, i.e., $\lambda \propto k_B T$. After annihilation of the kinks, the dislocation core occupies a transient unstable state. We can thus assume that the energy of that state decreases exponentially with time. A dimensional analysis shows that the transient state energy should then decrease as

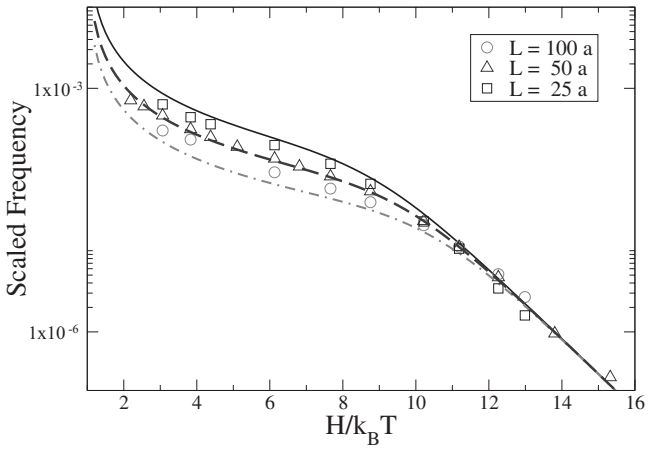

FIG. 8. Simulation data (symbols) for the normalized nucleation rate as a function of the activation ratio $H/k_B T$ for different dislocation lengths. The curves are predictions from Eq. (10).

$H \exp(-\lambda L_r t/m)$, where the length L_r is the spatial extent of the radiative segment and m is the atomic mass. The dislocation energy eventually reaches the thermal bath energy after a time on the order of $m \ln(H/k_B T)/\lambda L_r$, which we identify as the incubation time t_i. We thus have

$$t_i = \frac{A}{k_B T} \ln\left(\frac{H}{k_B T}\right), \tag{9}$$

where $A = 0.1722$ eV ps is adjusted to fit the maximum of the distribution functions of waiting times. Note that if we use Leibfried's expression, with parameters that correspond to bcc iron ($z=1$, $m=m_{\mathrm{Fe}}$, and $c_s = 2500$ m s^{-1}) and $L_r = 10a$ identified with the extension of the critical nucleus, we obtain $A = 0.06$ eV ps, which is of the same order of magnitude as the value fitted here.

We then express the average waiting time $\langle t_w \rangle$ as the sum of the incubation time t_i plus the thermally activated time; i.e., normal thermal activation starts after the incubation time. The scaled frequency $\tilde{\Gamma}$ becomes

$$\tilde{\Gamma} = \frac{1}{t_i \nu_D L/a + \exp(H/k_B T)}. \tag{10}$$

For the thermally activated time, we chose to keep the form of the exponential law proposed by Friedel [Eq. (5)] since it proved very efficient for the low-temperature regime. Some minor improvements could however be obtained by accounting for the Goldstone pre-exponential factor. The expression for $\tilde{\Gamma}$ in Eq. (10) is compared to the simulation data in Fig. 6 where it is reported as a dashed line. A remarkable agreement is obtained at all values of the activation ratio and for all stresses. It must be pointed out that the phenomenological law for t_i has been derived from the maximum of the waiting time distributions and therefore has not been adjusted to fit directly $\tilde{\Gamma}$.

We note in Fig. 6 a small scatter in the frequency of type II simulations at high temperature for different stresses. This dependence is included in the above model since, for a given value of the activation ratio $H/k_B T$, if the stress increases,

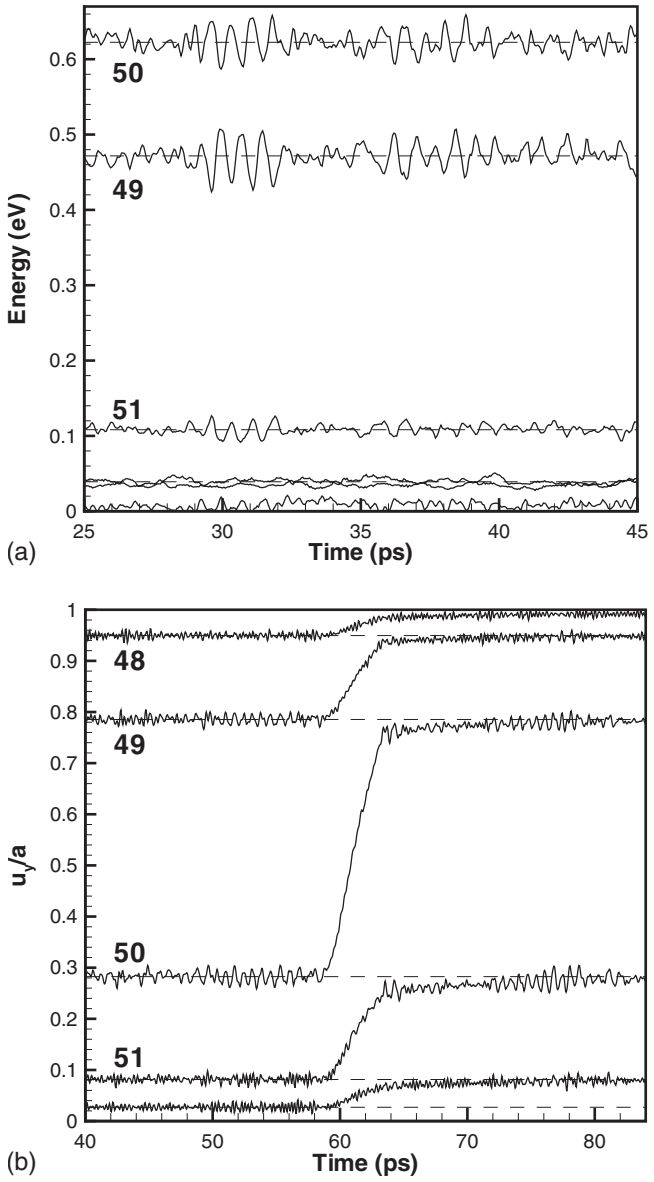

FIG. 9. (a) Average energy and (b) average Y displacement per row as a function of time. Row indices noted on the figure correspond to Fig. 1(b). In (b), a dislocation jump is shown. The dashed lines show equilibrium values. The data were obtained at 900 MPa and 200 K.

the enthalpy H decreases and thus the temperature T also decreases. Therefore, if the applied stress increases at fixed activation ratio, t_i increases from Eq. (9) and the jump frequency $\tilde{\Gamma}$ decreases from Eq. (10) as observed in Fig. 6. We also investigated the dependence of the jump frequency on the dislocation length L predicted by Eq. (9). Figure 8 shows the jump frequencies for different dislocation lengths along with the prediction of Eq. (9). In the low-temperature regime, all data fall on the same line, confirming the linear scaling of the exponential law on the dislocation length. On the other hand, at high temperature, we observe a scatter for the different lengths, which is well captured by the prediction of Eq. (9).

V. DISCUSSION

Figure 3 shows that the activation enthalpy for kink-pair nucleation obtained with the 2D-FK model, when properly scaled, agrees with the prediction of the (1+1)D-SG model as well as with experimental data. This *universal* behavior was already pointed out by Ngan and Zhang[51] who proposed a universal law of the form $0.1\mu b^3(1-\sigma/\sigma_P)^2$. This relation is a special case of the phenomenological law used here [Eq. (4)] which has been employed to model the experimental kink-pair nucleation enthalpy in bcc tantalum[49] and hcp zirconium[52] with parameters p and q slightly different from the ones obtained here but in the same range ($p=0.748$ and $q=1.172$ for Ta and $p=0.757$ and $q=1.075$ for Zr). Brünner and Diehl[47] also noted that the enthalpies obtained experimentally in bcc iron are well fitted by the (1+1)D-SG model.

The activation ratio H/k_BT controls the rate of kink-pair nucleation. The range considered here is between 4 and 16, which remains lower than the values obtained experimentally (typically 30; see Ref. 47), despite the fact that the time scale simulated here is much longer than in the 3D atomistic simulations. Depending on the activation ratio, we identified two regimes for the nucleation rate and thus for the dislocation velocity. In the low-temperature regime the end result does not depend on the type of simulations and follows an exponential law with an athermal prefactor. This scaling agrees very well with the relation proposed by Friedel[40] to describe the thermally activated velocity of dislocations. In the high-temperature regime, the dislocation velocity obtained for type I and type II simulations is slower than expected from the previous thermally activated law. For type I simulations the slowing down is limited and arises from the existence of a Goldstone mode.[23] For type II simulations, the high-temperature regime results from the existence of an incubation time after each annihilation of kinks. During which the dislocation cannot undergo a new jump. The physical origin of the incubation time is a recovery process of the dislocation core geometry. The incubation time decreases when the temperature increases [see Eq. (9)] because the strength of the phonon thermal bath increases, which accelerates the relaxation of the dislocation core. We believe that the suppression of the short waiting times is present at all activation ratios but can not be detected at low temperature because it is negligible compared to the thermally activated waiting time. Indeed, the incubation time increases only as the logarithm of activation ratio [see Eq. (9)] while the thermally activated term is exponential [see Eq. (6)]. The incubation time becomes visible in the distributions of waiting times (Fig. 7) only when it becomes of the same order as the average waiting time, which marks the transition between the low- and high-temperature regimes. It must be emphasized that the phenomenological analysis presented here for the incubation time remains very qualitative and a detailed treatment should be carried out to obtain a more accurate expression for the kink-pair nucleation rate at high temperatures.

As a summary, we employed a 2D-FK model in order to study the slow thermally activated motion of dislocations. For this, we computed independently the kink-pair nucleation rates using dynamical simulations and the kink-pair

nucleation enthalpies using static NEB simulations. For the low-temperature regime we confirm the accuracy of a transition state theory where the attempt frequency is simply taken as the vibration frequency of an elastic string at the bottom of a potential well. Interestingly, this law is valid even though the model includes nonlinear phenomena such as phonon modes localized near the dislocation line. We identified an unexpected high-temperature regime where dislocation motion is slower than the extrapolation from the low-temperature regime. It remains to be checked whether this high-temperature regime is a particularity of the FK model or if it can also be identified in 3D atomistic simulations. This work will be the subject of a future paper.

APPENDIX: INTERNAL DISLOCATION MODES

We report here our study of the vibrational modes of the dislocation in the course of finite temperature simulations. We first consider the dynamics of the atoms inside the dislocation core to show that the nonlinearities in the dislocation core imply a localized phonon mode, i.e., a vibrational mode extended along the dislocation line but localized in the transversal direction. Figure 9 presents the time variation of the average energy (potential plus kinetic) and average displacement for a few atomic rows near the dislocation core. Because of the thermal equilibrium, the kinetic energy is close to constant over time and is identical in each row such that the energy variations seen here are solely due to the potential energy. We see in Fig. 9(a) that in the dislocation core (rows 49 and 50 and to a lesser extent, row 51) the average energy undergoes well-defined oscillations while there is only thermal noise in the other rows. The vibrational mode is localized in the sense that the oscillations in rows 49 and 50 are out of phase and the energy is exchanged between these two rows and seems not to propagate in the rest of the crystal. To better analyze this localized mode, we computed the energy correlation function in rows inside and outside the dislocation core. The expression used is[53]

$$C(\tau) = \left\langle \frac{\langle E(t)E(t+\tau)\rangle - \langle E(t)\rangle\langle E(t+\tau)\rangle}{\langle E^2(t)\rangle - \langle E(t)\rangle\langle E^2(t)\rangle} \right\rangle, \qquad \text{(A1)}$$

where the inner brackets are time averages and the outer brackets average over a given row (row 50 inside the dislocation core and row 25 outside). The result is shown in Fig. 10. Outside the core [Fig. 10(b)], the correlation progressively decreases, with time while inside the core [Fig. 10(b)] there is a peak at 0.7 ps that corresponds to the characteristic period of the oscillations visible in Fig. 9(a). Note that since the displacements and energies shown here are averaged over

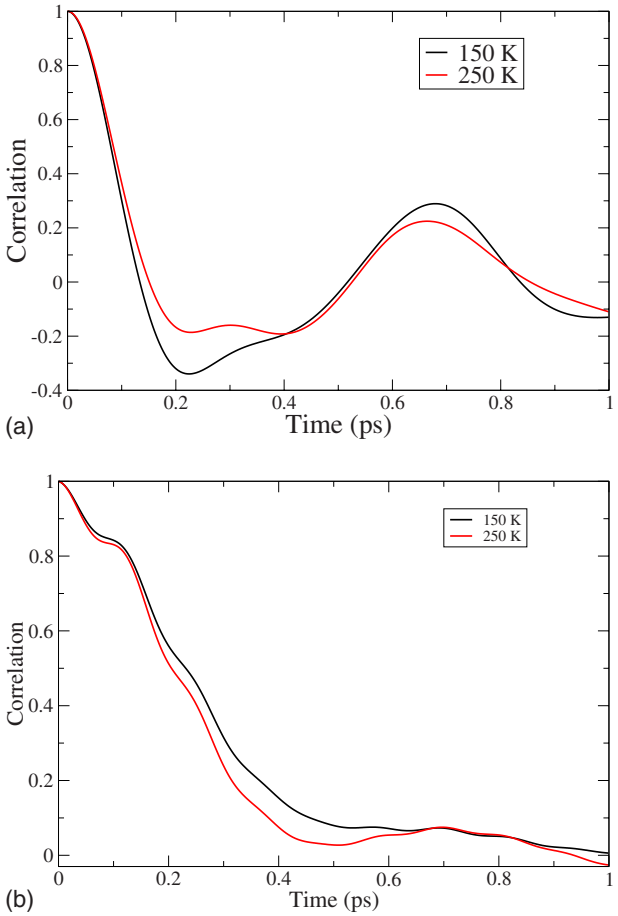

FIG. 10. (Color online) Energy correlation functions (a) inside and (b) outside the dislocation core. The applied stress is 900 MPa and two temperatures are considered: 150 and 250 K.

atomic rows, the oscillations are correlated in the Y direction. The associated mode has thus a short extension outside the core but has a long wavelength inside the core. Such localized phonon modes have been observed by Gornostyrev *et al.*[35] and were predicted by Weiner.[54,55]

From Fig. 9(b), which includes a jump event, following the average trajectory of rows 50 and 51, one sees that just after the dislocation jump, around 64 ps, the mean positions of the rows differ from the static equilibrium ones (horizontal dashed lines). After 10–20 ps, the mean positions become equal to the static ones. During this recovery process, no kink-pair nucleates. The time required for repositioning the dislocation core is clearly at the origin of the delay in the nucleation rate discussed in Sec. IV.

[1] R. Peierls, Proc. Phys. Soc. London **52**, 34 (1940).
[2] P. Guyot and J. Dorn, Can. J. Phys. **45**, 983 (1967).
[3] M. Duesbery, Philos. Mag. **19**, 501 (1969).
[4] H. Alexander, in *Dislocations in Solids*, edited by F. Nabarro (North-Holland, Amsterdam, 1986), Vol. 8, p. 115.
[5] V. Vitek, Cryst. Lattice Defects **5**, 1 (1974).
[6] L. Kubin, Rev. Deform. Behav. Mater. **1**, 244 (1977).
[7] A. Seeger, Philos. Mag. **1**, 651 (1956).
[8] M. Peyrard and T. Dauxois, *Physics of Solitons* (Cambridge University Press, Cambridge, England, 2006).

[9] M. Büttiker and R. Landauer, Phys. Rev. Lett. **43**, 1453 (1979).
[10] M. Büttiker and R. Landauer, Phys. Rev. A **23**, 1397 (1981).
[11] P. Hänggi, F. Marchesoni, and P. Sodano, Phys. Rev. Lett. **60**, 2563 (1988).
[12] F. Marchesoni, Phys. Rev. Lett. **73**, 2394 (1994).
[13] M. Büttiker and T. Christen, Phys. Rev. Lett. **75**, 1895 (1995).
[14] J. Frenkel and T. Kontorova, J. Phys. (Moscow) **1**, 137 (1939).
[15] T. Munakata, Phys. Rev. A **45**, 1230 (1992).
[16] F. J. Alexander and S. Habib, Phys. Rev. Lett. **71**, 955 (1993).
[17] S. Habib and G. Lythe, Phys. Rev. Lett. **84**, 1070 (2000).
[18] F. Marchesoni, C. Cattuto, and G. Costantini, Phys. Rev. B **57**, 7930 (1998).
[19] A. I. Bochkarev and P. de Forcrand, Phys. Rev. Lett. **63**, 2337 (1989).
[20] M. Alford, H. Feldman, and M. Gleiser, Phys. Rev. Lett. **68**, 1645 (1992).
[21] A. Seeger and P. Schiller, in *Physical Acoustics*, edited by W. Mason (Academic, New York, 1966), Vol. III.
[22] V. Celli, M. Kabler, T. Ninomiya, and R. Thomson, Phys. Rev. **131**, 58 (1963).
[23] J. F. Currie, J. A. Krumhansl, A. R. Bishop, and S. E. Trullinger, Phys. Rev. B **22**, 477 (1980).
[24] J. Marian, W. Cai, and V. Bulatov, Nat. Mater. **3**, 158 (2004).
[25] C. Domain and G. Monnet, Phys. Rev. Lett. **95**, 215506 (2005).
[26] J. Chaussidon, M. Fivel, and D. Rodney, Acta Mater. **54**, 3407 (2006).
[27] D. Rodney, Phys. Rev. B **76**, 144108 (2007).
[28] J. Moriarty, V. Vitek, V. Bulatov, and S. Yip, J. Comput.-Aided Mater. Des. **9**, 99 (2002).
[29] C. Woodward and S. I. Rao, Phys. Rev. Lett. **88**, 216402 (2002).
[30] L. Ventelon, F. Willaime, and P. Leyronnas (unpublished).
[31] M. Duesbery, Philos. Mag. **31**, 1747 (1983).
[32] L. Pizzagalli, A. Pedersen, A. Arnaldsson, H. Jónsson, and P. Beauchamp, Phys. Rev. B **77**, 064106 (2008).
[33] M. Duesbery and Z. Basinski, Acta Metall. Mater. **41**, 643 (1993).
[34] Y. N. Gornostyrev, M. I. Katsnelson, A. V. Kravtsov, and A. V. Trefilov, Phys. Rev. B **60**, 1013 (1999).
[35] Y. N. Gornostyrev, M. I. Katsnelson, A. V. Kravtsov, and A. V. Trefilov, Phys. Rev. E **66**, 027201 (2002).
[36] B. Joos, Solid State Commun. **42**, 709 (1982).
[37] H. Jónsson, G. Mills, and K. Jacobsen, in *Classical and Quantum Dynamics in Condensed Phase Simulations*, edited by G. Berne and D. Coker (World Scientific, Singapore, 1998), p. 385.
[38] W. Press, S. Teukolsky, W. Vetterling, and B. Flannery, *Numerical Recipes* (Cambridge University Press, Cambridge, England, 1996).
[39] G. Vineyard, J. Phys. Chem. Solids **3**, 121 (1957).
[40] J. Friedel, *Dislocations* (Pergamon, London, 1964).
[41] G. Ackland, D. Bacon, A. Calder, and T. Harry, Philos. Mag. A **75**, 713 (1997).
[42] M. Allen and D. Tildesley, *Computer Simulation of Liquids* (Oxford University Press, Oxford, 1987).
[43] H. Andersen, J. Chem. Phys. **72**, 2384 (1980).
[44] J. Eshelby, Proc. R. Soc. London, Ser. A **266**, 222 (1962).
[45] A. H. W. Ngan and M. Wen, Phys. Rev. Lett. **87**, 075505 (2001).
[46] Y. Aono, E. Kuramoto, and K. Kitajima, *Dislocation Dynamics and Plasticity* (Springer, Berlin, 1991), p. 94.
[47] D. Brünner and J. Diehl, Phys. Status Solidi A **124**, 455 (1991).
[48] U. Kocks, A. Argon, and M. Ashby, in *Progress in Materials Science*, edited by B. Chalmers, J. Christian, and T. Massalski (Pergamon, Oxford, 1975), Vol. 19.
[49] M. Tang, L. Kubin, and G. Canova, Acta Mater. **46**, 3221 (1998).
[50] G. Leibfried, Z. Phys. **127**, 344 (1950).
[51] A. Ngan and H. Zhang, J. Appl. Phys. **86**, 1236 (1999).
[52] G. Monnet, B. Devincre, and L. Kubin, Acta Mater. **52**, 4317 (2004).
[53] R. Reigada, A. Romero, A. Sarmiento, and K. Lindenberg, J. Chem. Phys. **111**, 1373 (1999).
[54] J. Weiner and W. Sanders, Phys. Rev. **134**, A1007 (1964).
[55] J. Weiner, Phys. Rev. **136**, A863 (1964).